

Article

Influence Mechanism of Geometric Characteristics of Water Conveyance System on Extreme Water Hammer during Load Rejection in Pumped Storage Plants

Sheng Chen ^{1,*}, Jian Zhang ¹, Gaohui Li ² and Xiaodong Yu ^{1,*}

¹ College of Water Conservancy and Hydropower Engineering, Hohai University, Nanjing 210098, China

² Powerchina Huadong Engineering Corporation Limited, Hangzhou 311122, China

* Correspondence: chensheng@hhu.edu.cn (S.C.); yuxiaodong_851@hhu.edu.cn (X.Y.);

Tel.: +86-25-8378-7313 (S.C. & X.Y.)

Received: 24 June 2019; Accepted: 23 July 2019; Published: 24 July 2019



Abstract: Pumped storage plants (PSPs) have achieved rapid development and deployment worldwide since the penetration of intermittent renewable energy sources (RES). Hydraulic transient analysis in the PSP, to obtain the control parameters such as extreme water hammer pressure, is vital to the safe design of water conveyance system. Empirically, simultaneous load rejection (SLR) is commonly accepted as the control condition for extreme water hammer, while it is not completely true for the PSP. Employing theoretical analysis and numerical simulation, this study systematically investigates the effects of geometric characteristics on the extreme water hammer, and reveals the mechanism leading to the maximum spiral case pressure (SCP) during a two-stage load rejection (TLR) process. The results indicate that the extreme water hammer pressure is closely related to geometric characteristics of the water conveyance system, performing the allocation of the water inertia time constant of the main and branch pipelines. When the water inertia time constant in the branch pipe is dominant ($\tau_{11} > 0.24$ for example), the maximum SCP will occur in TLR conditions rather than SLR. Moreover, the maximum SCP is almost the same, providing the water inertia time constants of both the main and branch pipelines are kept constant.

Keywords: pumped storage plant; transient analysis; simultaneous load rejection; two-stage load rejection; geometric characteristic; water conveyance system; water inertia time constant

1. Introduction

In recent years, the penetration of renewable energy sources (RES) have increased rapidly worldwide due to the ever-increasing environmental concerns and electricity demand [1,2]. Compared with traditional fossil fuels, RES are regarded as sustainable, clean, low-carbon, and economical energy sources [3]. However, the unpredictable and intermittent nature of some RES—such as wind, solar, and wave energy—brings significant challenges to the grid's security, stability, reliability, and efficiency [4–6]. To solve the above problems caused by the intermittency of RES, energy storage technology is an effective way forward. Among the available technologies, the pumped storage plant (PSP) is proven to be the most mature, cost-effective, and large-scale one, considered to be an essential part of a renewable oriented power system [7]. Therefore, PSPs have broad prospects and are developing rapidly in worldwide.

A PSP usually has the functions of peak shaving, valley filling, frequency modulation, phase modulation, and accident standby in the electric grid system [8,9]. To fulfill these regulatory functions, the PSP working conditions change frequently and the reversible pumped turbines switch rapidly between the pump mode and turbine mode, substantially increasing the probability of load rejection.

The following severe water hammer caused by emergency closure of guide vanes may result in serious threat to the safe operation of the water conveyance system. Therefore, hydraulic transient analysis on the water hammer phenomenon of PSPs is an important and essential work, to provide safe and optimal operation, during the design or service stage. This has been extensively studied, both numerically and experimentally. The general theory of water hammer was first developed by Allievi [10]. Further efforts by Wood [11], Rich [12], Parmakian [13], Streeter and Lai [14], and Streeter and Wylie [15] formed the classical mass and momentum equations for one-dimensional water hammer flows, which were then written in numerous classical textbooks for transient flow analysis [16,17]. The above-mentioned governing equations formed a pair of quasi-linear hyperbolic partial differential equations, which could seldom be solved analytically. Therefore, various numerical approaches have been introduced for calculation of the pipeline transients, including the method of characteristics (MOC) [16,17], wave plan method [18], finite volume method [19], finite element method, and finite difference method [20]. Later, these theoretical and numerical approaches were widely applied in hydroelectrical power systems. Yang et al. [21] presented a mathematical model of the hydroelectrical power system based on TOPSYS, as well as its application. Employing MOC, sensitivity analysis of hydraulic transient at runaway and the interaction effect of hydraulic transient flow for two parallel reversible pump turbines (RPTs) have been numerically investigated by Rezghi and Riasi [22,23]. Hu et al. [24] conducted transient simulation and analyzed the transient pressure pulsations characteristics of the RPT under load rejection. Zhou et al. [25] proposed a 3D numerical method based on single-phase and volume of fluid (SP-VOF) to investigate the transient characteristics of a PSP. Fu et al. [26,27] employed a dynamic mesh technology to simulate the flow behavior in an RPT under load rejection, and the energy transformation and flow mechanism were analyzed as well. Different innovative closure schemes are proposed by Kuwabara et al. [28] and Yu et al. [29], respectively, which can effectively mitigate the water hammer due to S-shaped characteristics. Applying the method of internal characteristics, the combined closing scheme of ball valve and wicket gate during load rejection was simulated by Li et al. [30]. Zhang et al. [31] simulated the load rejections of Tongbai PSP in China, and the results agreed well with the field test data. Chen et al. [32] calibrated the boundary conditions based on field tests and gave the numerical prediction of the extreme water hammer pressure under critical load case scenarios.

Reliable prediction of the hydraulic parameters, including maximum spiral case pressure (SCP) and minimum draft tube pressure (DTP), is of great importance for the safe design of the water conservancy. Empirically, simultaneous load rejection (SLR) is usually considered to be the critical load case scenario, in which extreme values of SCP or DTP occur. This is true for conventional hydropower plant with Francis turbines in most cases. For the PSP, however, it is not the case due to the well-known S-shaped characteristics of the RPTs, which is contributed to by the runner design of focusing on pump mode [33]. The hydraulic behavior during load rejection of the PSP is more complicated and distinct from the conventional hydroelectric power plant. Recent studies indicated that extreme low DTP may occur in a specific load case scenario, namely TLR, which was firstly proposed by Yokoyama and Shimmei [34] to study the dynamic characteristics of RPTs in the PSP. TLR usually happens in the system layout of multiple RPTs sharing the same main pipe, resulting from the hydraulic disturbance. The RPT rejecting the load firstly can increase the working head of the other RPTs through the hydraulic connection provided by the bifurcations or trifurcations. Then, the overloaded units may reject the load in turn, defined as TLR (Figure 1) [35]. Currently, TLR is extensively investigated in PSPs with concerns for the minimum DTP. Zhang and Suo [36] first found the minimum pressure of the draft tube may occur during TLR when discussing the setting criterion for tailrace surge tank. Subsequently, Zhang et al. [37,38] conducted a series of studies on TLR, and concluded that the unique S-shaped characteristics of RPT were responsible for the abnormal low DTP, and the downstream pipeline layout had great influence on the magnitude of DTP. By theoretical analysis and numerical simulation, Zeng et al. studied the impact of the pipe diameters on DTP [39], proposed several multiphase closing schemes to mitigate the severe water hammer and rotational speed rise under TLR [40], and explained

the physical mechanism of the phenomenon leading to extreme low DTP [41]. In order to control the great pressure drop in the draft tube, several possible countermeasures were proposed by Fang and Koutnik [42].

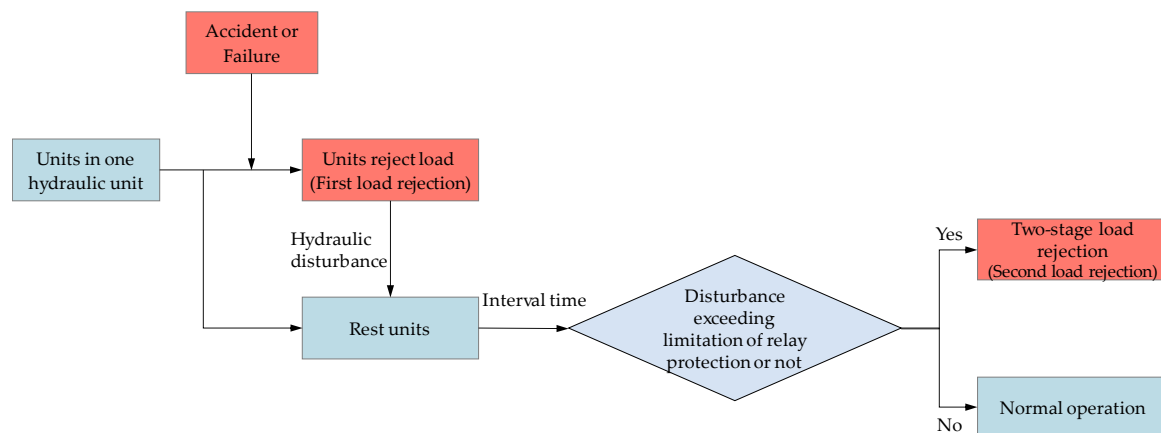


Figure 1. Schematic diagram of two-stage load rejection.

The above achievements confirm that TLR is the exact critical load case scenario for minimum DTP, which was ascribed to the S-shaped characteristics and the layout of water conveyance system. For maximum SCP, however, TLR can also sometimes be the critical load case rather than SLR [43]. If the extreme water hammer appears in TLR, but is not considered in advance, the unavoidable extreme pressure may result in serious damage to the system. In fact, the extreme water hammer pressure, no matter SCP or DTP, also greatly depends on the geometric characteristic of the water conveyance system, including the diameter and length of the pipelines. Different geometric dimensions of the main and branch pipes may result in the extreme water hammer pressure occurring in different load cases, TLR or SLR. However, the comprehensive influence analysis of geometric characteristics of the water conveyance system on extreme water hammer are obviously limited. How the geometric characteristics affect the extreme water hammer pressure is still unclear. Therefore, an in-depth and systematic study on extreme water hammer during load rejection of different geometric characteristics of water conveyance system is required, especially for the maximum SCP.

The present study investigates the influence mechanism of geometric characteristics of water conveyance system on extreme water hammer during load rejection in the PSP. Rigid water hammer theory and the numerical model for hydraulic transients based on MOC are employed to illustrate how the geometric characteristics affect the extreme water hammer pressure, such as the maximum SCP.

2. Theoretical Analysis and Mathematical Model

2.1. Theoretical Analysis

The schematic diagram for a typical PSP with two RPT units is shown in Figure 2. RPT 1 and 2 are symmetrically arranged to obtain the best flow conditions, and the initial outputs are the same. As mentioned previously, RPT 1 and RPT 2 share the same headrace tunnel (number 1), thereby RPT 1 rejecting the full load may result in the subsequent load rejection of RPT 2. Rigid water column theory [16,17] is employed for the following quantitative analysis.

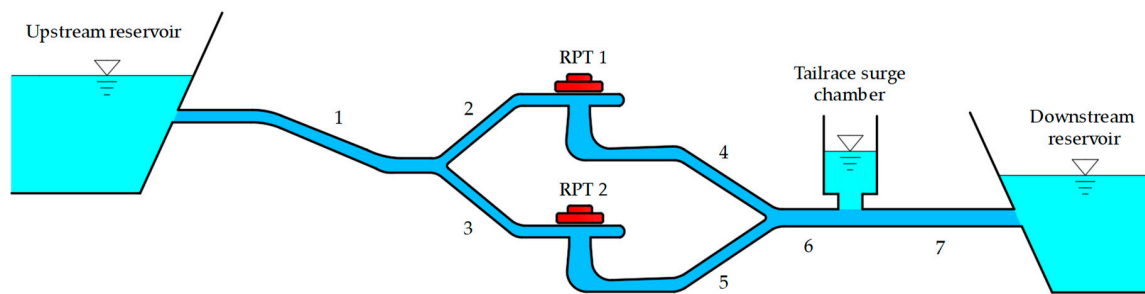


Figure 2. Schematic of a typical pumped storage plant system.

With reference to Figure 2, the momentum equations [16,17] of this hydraulic system are given by

$$\frac{L_1}{gf_1} \frac{dQ_T}{dt} = Z_u - \alpha_1 Q_T^2 - H_{Fu} \quad (1)$$

$$\frac{L_2}{gf_2} \frac{dQ_1}{dt} = H_{Fu} - \alpha_2 Q_1^2 - H_{tu1} \quad (2)$$

$$\frac{L_3}{gf_3} \frac{dQ_2}{dt} = H_{Fu} - \alpha_3 Q_2^2 - H_{tu2} \quad (3)$$

where L_i and f_i ($i = 1-3$) are length and cross-sectional area of the i -th pipeline reach, respectively; α_i ($i = 1-3$) is head loss coefficient of the i -th reach; Z_u is the upstream reservoir water level; H_{tu_j} ($j = 1-2$) is the head at the spiral case of the j -th RPT, respectively; H_{Fu} is the head at upstream bifurcation node; Q_T is headrace tunnel discharge; Q_1 and Q_2 are the demand discharges of RPT 1 and RPT 2, respectively; t is time; and g is gravitational acceleration.

The continuity equation [16,17] is

$$Q_T = Q_1 + Q_2 \quad (4)$$

Taking Equations (1) and (2) simultaneously gives

$$\frac{L_1}{gf_1} \frac{dQ_T}{dt} + \frac{L_2}{gf_2} \frac{dQ_1}{dt} = Z_u - \alpha_1 Q_T^2 - \alpha_2 Q_1^2 - H_{tu1}. \quad (5)$$

After transformation, Equation (5) takes the form

$$H_{tu1} = Z_u - \alpha_1 Q_T^2 - \alpha_2 Q_1^2 - \left(\frac{L_1}{gf_1} \frac{dQ_T}{dt} + \frac{L_2}{gf_2} \frac{dQ_1}{dt} \right). \quad (6)$$

Substitution of Equation (4) into Equation (6) yields

$$H_{tu1} = Z_u - \alpha_1 Q_T^2 - \alpha_2 Q_1^2 - \left(\frac{L_1}{gf_1} + \frac{L_2}{gf_2} \right) \frac{dQ_1}{dt} - \frac{L_1}{gf_1} \frac{dQ_2}{dt}. \quad (7)$$

In the same manner for RPT 2

$$\begin{aligned} H_{tu2} &= Z_u - \alpha_1 Q_T^2 - \alpha_3 Q_2^2 - \left(\frac{L_1}{gf_1} \frac{dQ_T}{dt} + \frac{L_3}{gf_3} \frac{dQ_2}{dt} \right) \\ &= Z_u - \alpha_1 Q_T^2 - \alpha_3 Q_2^2 - \left(\frac{L_1}{gf_1} + \frac{L_3}{gf_3} \right) \frac{dQ_2}{dt} - \frac{L_1}{gf_1} \frac{dQ_1}{dt} \end{aligned} \quad (8)$$

Equations (7) and (8) indicate that the SCP (H_{tu1} and H_{tu2}) are affected by the following parameters: The upstream reservoir water level (Z_u), discharge of headrace tunnel (Q_T), discharge of corresponding branch pipelines (Q_1 or Q_2), geometric characteristics of upstream water conveyance system (L_i and f_i , $i = 1-3$), head loss of each reaches ($\alpha_1 Q_T^2$, $\alpha_2 Q_1^2$, and $\alpha_3 Q_2^2$), and the rate of discharge change ($\frac{dQ_1}{dt}$ and $\frac{dQ_2}{dt}$). The SCP of RPT 1 (or RPT 2) is related not only to the characteristics of the branch pipe RPT

1 (or RPT 2) location, but is also related to that of the common shared main pipe. Obviously, the critical terms are $\frac{L_1}{gf_1} \frac{dQ_T}{dt}$ and $\frac{L_3}{gf_3} \frac{dQ_2}{dt}$.

During SLR, Equation (8) can be written as

$$H_{tu2 \text{ SLR}} = Z_u|_{\text{SLR}} - \alpha_1 Q_T^2|_{\text{SLR}} - \alpha_3 Q_2^2|_{\text{SLR}} - \frac{L_1}{gf_1} \frac{dQ_T}{dt}|_{\text{SLR}} - \frac{L_3}{gf_3} \frac{dQ_2}{dt}|_{\text{SLR}}. \quad (9)$$

As for TSL, assuming RPT 1 firstly rejects full load by emergency closure, then RPT 2 commits full load rejection after a certain interval of time (similarly hereinafter). Equation (8) takes the form

$$H_{tu2 \text{ TLR}} = Z_u|_{\text{TLR}} - \alpha_1 Q_T^2|_{\text{TLR}} - \alpha_3 Q_2^2|_{\text{TLR}} - \frac{L_1}{gf_1} \frac{dQ_T}{dt}|_{\text{TLR}} - \frac{L_3}{gf_3} \frac{dQ_2}{dt}|_{\text{TLR}}. \quad (10)$$

Due to the same initial condition of a load case,

$$Z_u|_{\text{TLR}} = Z_u|_{\text{SLR}}, \quad \alpha_1 Q_T^2|_{\text{SLR}} = \alpha_1 Q_T^2|_{\text{TLR}}, \quad \alpha_3 Q_2^2|_{\text{SLR}} = \alpha_3 Q_2^2|_{\text{TLR}}.$$

By use of Equation (10) minus Equation (9) to eliminate duplicate parameters, it becomes

$$H_{tu2 \text{ TLR}} - H_{tu2 \text{ SLR}} = \frac{L_1}{gf_1} \left(-\frac{dQ_T}{dt}|_{\text{TLR}} + \frac{dQ_T}{dt}|_{\text{SLR}} \right) + \frac{L_3}{gf_3} \left(-\frac{dQ_2}{dt}|_{\text{TLR}} + \frac{dQ_2}{dt}|_{\text{SLR}} \right). \quad (11)$$

Defining the following dimensionless parameters

$$h = \frac{H}{H_r}, \quad z = \frac{Z}{H_r}, \quad q = \frac{Q}{Q_r} \quad (12)$$

where the subscript r indicates the rated quantities.

Then, the Equations (8) and (11) are transformed into

$$\begin{aligned} h_{tu2} &= z_u - \frac{\alpha_1 Q_r^2}{H_r} q_T^2 - \frac{\alpha_3 Q_r^2}{H_r} q_2^2 - \left(T_{wm,u} \frac{dq_T}{dt} + T_{wb,u} \frac{dq_2}{dt} \right) \\ &= z_u - \frac{\alpha_1 Q_r^2}{H_r} q_T^2 - \frac{\alpha_3 Q_r^2}{H_r} q_2^2 - T_{w,u} \frac{dq_2}{dt} - T_{wm,u} \frac{dq_1}{dt} \end{aligned} \quad (13)$$

$$h_{tu2 \text{ TLR}} - h_{tu2 \text{ SLR}} = T_{wm,u} \left(-\frac{dq_T}{dt}|_{\text{TLR}} + \frac{dq_T}{dt}|_{\text{SLR}} \right) + T_{wb,u} \left(-\frac{dq_2}{dt}|_{\text{TLR}} + \frac{dq_2}{dt}|_{\text{SLR}} \right) \quad (14)$$

where $T_{wm,u} = \frac{L_1 Q_r}{gf_1 H_r}$ and $T_{wb,u} = \frac{L_2 Q_r}{gf_2 H_r}$ are water inertia time constant of upstream main pipe and upstream branch pipes, respectively; $T_{w,u} = T_{wm,u} + T_{wb,u}$ is water inertia time constant of upstream pipelines.

For Equation (14), if $h_{tu2 \text{ TLR}} - h_{tu2 \text{ SLR}} < 0$, the extreme SCP will occur in SLR. Otherwise, it will occur during TLR. Figure 3 gives the general law of the wicket gates opening, and discharge process of main and branch pipes during SLR and TLR, respectively. As shown in Figure 3, the total closure time of wicket gates for SLR is t_4 , while that for TLR is $t_5 (= t_4 + t_c)$. That is to say, TLR is equivalent to extending the total closure time of the system compared with SLR. Finally, the times for the main pipe discharge dropping to the first valley under SLR and TLR are t_1 and t_2 , respectively, which results in the decrease of the flow gradient in main pipeline. It is obvious that $\frac{dQ_T}{dt}|_{\text{SLR}} < 0$ when $t < t_1$, and $\frac{dQ_T}{dt}|_{\text{TLR}} < 0$ when $t < t_2$. Additionally, the instant for maximum SCP during SLR is less than t_1 , and that during TLR is less than t_2 . Thus, there exists $\left(-\frac{dQ_T}{dt}|_{\text{TLR}} + \frac{dQ_T}{dt}|_{\text{SLR}} \right) < 0$ or $\left(-\frac{dq_T}{dt}|_{\text{TLR}} + \frac{dq_T}{dt}|_{\text{SLR}} \right) < 0$ for main pipe. This factor makes the maximum SCP under TLR less severe than SLR, and also explains why TLR has been paid little attention during transient calculation. While for the branch pipe numbered 3, it also takes t_1 for the discharge to drop to the first valley during SLR. However, the load rejection of RPT 1 inevitably increases the demand discharge of RPT 2, which will be dropped to the first valley at

a greater rate of discharge change in a shorter time ($t_3 - t_c$). As a result, the flow gradient of the branch pipe of RPT 2 is much greater than SLR, namely $\left(-\frac{dQ_2}{dt}\Big|_{TLR} + \frac{dQ_2}{dt}\Big|_{SLR}\right) > 0$ or $\left(-\frac{dq_2}{dt}\Big|_{TLR} + \frac{dq_2}{dt}\Big|_{SLR}\right) > 0$. Therefore, Equation (14) is not necessarily negative as it is on the surface. That is, it is not always the case that the maximum SCP during TLR is less than that during SLR.

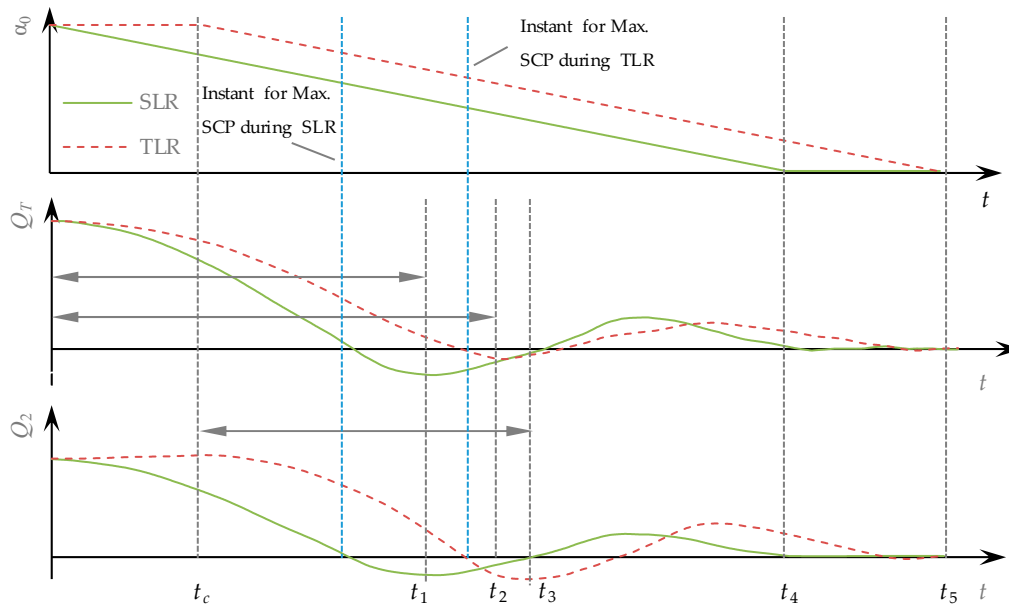


Figure 3. Schematic of wicket gate opening, discharge of the main and branch pipes during simultaneous load rejection (SLR) and two-stage load rejection (TLR).

In fact, the sign of Equation (14) also greatly depends on the geometric characteristics of upstream water conveyance system, such as L_i and f_i ($i = 1-3$). If the headrace tunnel is long enough and the area is appropriate, the term of L_1/f_1 (or $T_{wm,u}$) will be large enough. The water inertia in the main pipeline becomes the dominant factor, thereby maximum SCP will occur during the load case of SLR. Conversely, if the proportion of the branch pipe length is larger and the corresponding area is relatively small to make L_3/f_3 large enough, namely $T_{wb,u}$ large enough, the water inertia of the branch pipe will be the dominant factor. At this point, the maximum SCP following TLR will be greater than that of SLR.

In summary, the maximum SCP during load rejection is greatly affected by the geometric characteristics of the water conveyance system. When the water inertia time constant in the branch pipeline is dominant, the extreme water hammer will occur under TLR condition. In addition, ignoring the influence of head loss, if the water inertia time constants of both main and branch pipelines are kept constant by changing the lengths and diameters simultaneously, the discharge change rate ($\frac{dq_T}{dt}$, $\frac{dq_1}{dt}$ and $\frac{dq_2}{dt}$) will remain unchanged, and the extreme water hammer will as well.

2.2. Mathematical Model

Since MOC is a reliable and effective method for hydraulic transient analysis [35,44], it is employed to simulate hydraulic transients during load rejection. The basic equations of motion and continuity for the pressurized conduits could be referred to in the literature [16,17], as well as the boundary conditions, such as the reservoirs, series connections, junctions, and surge tanks. The key boundary condition of the RPT and the transformation of the RPT characteristics are given herein.

2.2.1. Basic Equations of RPT

An RPT is the vital component for the PSP system. The basic equations include the head balance equation and speed change equation. Figure 4 gives the sketch of the boundary condition of the RPT, and the head balance equation can be expressed as

$$H = \left(H_{tu} + \frac{|Q|Q}{2gf_{sc}^2} \right) - \left(H_{td} + \frac{|Q|Q}{2gf_{dt}^2} \right) \quad (15)$$

in which f_{sc} is the area at spiral case end; f_{dt} is the area at draft tube inlet; and Q is demand discharge of the RPT.

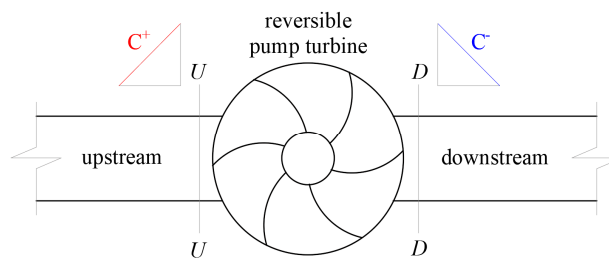


Figure 4. Sketch of reversible pump turbines (RPT) in pipeline.

The speed change in terms of the power produced by the RPT is

$$P - P_G = I\omega \frac{d\omega}{dt} \quad (16)$$

$$I = WR_g^2/g$$

where P is the power generated by the RPT; P_G is the power absorbed by the generator; ω is the angular velocity; $d\omega/dt$ is the angular acceleration; I is the polar moment of inertia of rotating fluid and mechanical parts; R_g is gyration radius; W is the weight.

The RPT unit will be disconnected from the grid as soon as load rejection occurs, thereby $P_g = 0$. The guide vanes are subsequently closed emergently by the given closure law to prevent overspeed of the rotational speed. By integration and Taylor expansion, Equation (16) is transferred to algebraic equations, given by

$$n = n_0 + \frac{\Delta t}{2T_a}(\beta + \beta_0) \quad (17)$$

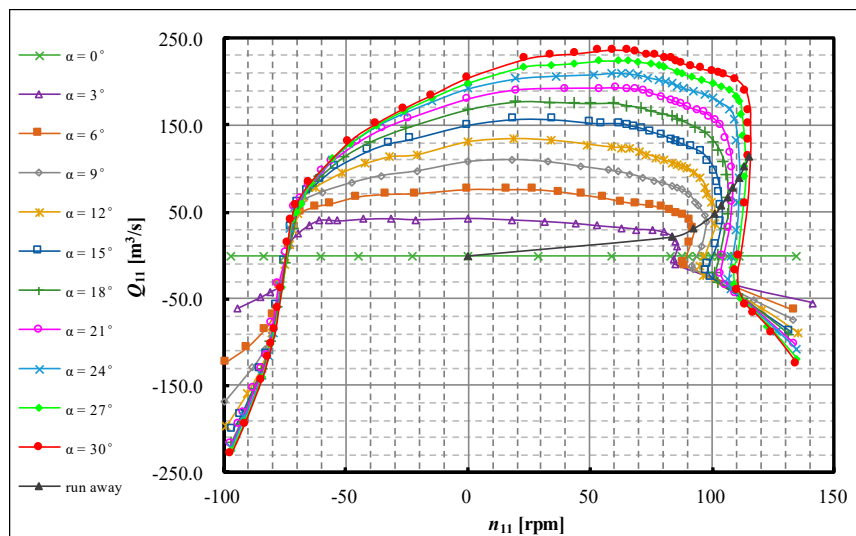
in which n ($= N/N_r$) and β ($= M/M_r$) are dimensionless rotational speed and dimensionless torque, respectively; n_0 and β_0 are the calculation results of a previous time step of n and β , respectively; T_a is inertia time constant of the RPT units, defined as $T_a = \frac{GD^2|N_r|}{374.7M_r}$, with N_r rated rotational speed and M_r rated torque; and Δt is time step.

2.2.2. Modified Suter Transformation for RPT Characteristics

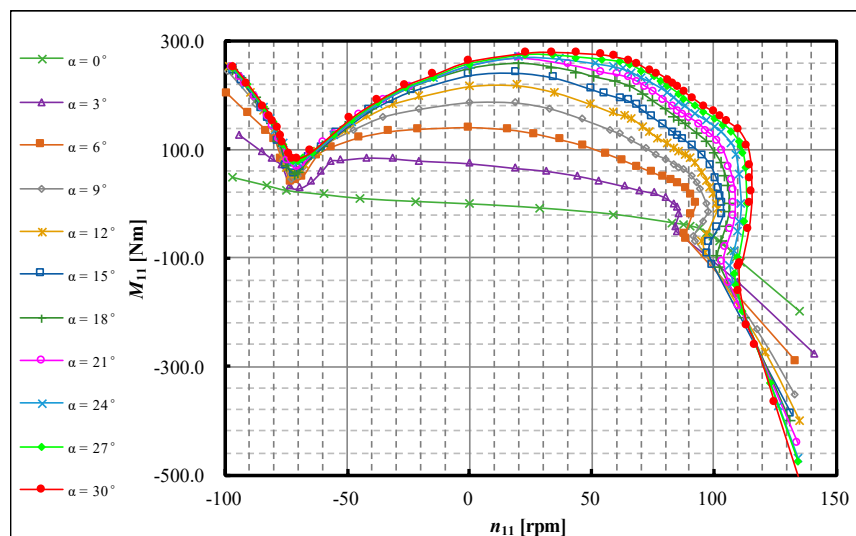
The hydraulic behavior of an RPT is usually described with two four-quadrant characteristics curves, including a series of guide vane opening curves (as shown in Figure 5). The characteristics curves are depicted by the unit rotational speed n_{11} , unit discharge Q_{11} , unit torque M_{11} , and guide vane opening α_0 , which are defined as follows

$$n_{11} = \frac{nD}{\sqrt{H}} \quad Q_{11} = \frac{Q}{D^2\sqrt{H}} \quad M_{11} = \frac{M}{D^3H} \quad (18)$$

where D is runner diameter of the RPT.



(a)



(b)

Figure 5. Four-quadrant characteristics of the RPT: (a) $Q_{11} \sim n_{11}$; (b) $M_{11} \sim n_{11}$.

On the characteristics curves of RPTs, there is a zone known as S-shape region, where three unit flows or torques exist at a given unit speed. Such a multi-valued nature will pose great difficulty in the interpolation of these curves during the transient simulation. Herein, a modified Suter transform [45] is applied for the mathematic model to overcome this challenge.

$$WH(x, y) = \frac{1}{(Q_{11}/Q_{11r} + c)^2 + (n_{11}/n_{11r})^2} \tag{19}$$

$$WM(x, y) = M_{11}/M_{11r} \tag{20}$$

$$\begin{cases} x = \tan^{-1}[(Q_{11}/Q_{11r} + c)/(n_{11}/n_{11r})], & n_{11}/n_{11r} \geq 0 \\ x = \pi + \tan^{-1}[(Q_{11}/Q_{11r} + c)/(n_{11}/n_{11r})], & n_{11}/n_{11r} < 0 \end{cases} \tag{21}$$

in which WH is the discharge function; WM is the torque function; x is the polar angle, determined by Equation (21); y is the dimensionless guide vane opening; and c is a constant, usually selected between 1.0 to 1.5. The subscript r denotes the rated values. Through the use of the modified

Suter transformation, the characteristics of RPT can be turned as the *WH* and *WB* curves, which are single-valued with the polar angle x .

2.2.3. Technical Parameters

One PSP located in China is used for numerical simulation. Figure 2 depicts its simplified layout. The installed capacity of the PSP is 1200 MW, with four identical RPTs. Each RPT can develop 306.1 MW in rated turbine operation. There are two hydraulic units, in which two RPTs share a common headrace tunnel. The normal water levels of upstream and downstream reservoirs are 815.5 m and 413.5 m, respectively. The dead water levels of upstream and downstream reservoirs are 782.0 m and 383.0 m, respectively. The rated discharge $2 \times 86.68 \text{ m}^3/\text{s}$, rated speed is 375.0 r/m, rated head is 400.0 m, maximum head is 432.47 m, and minimum head is 361.08 m. As shown in Figure 5, the pump-turbines have pronounced S-shaped region. The parameters of the conduits are listed in Table 1. The guide vanes are closed down linearly in 26 s.

Table 1. Parameters of water conveyance system.

Number of Reaches	Length L (m)	Diameter D (m)	Head Loss Coefficient α ($\times 10^{-6}$) (l)	Initial Demand Discharge (m^3/s)
1	1200	6.8	123.24	162.42
2	120	2.8	781.80	81.21
3	120	2.8	781.80	81.21
4	200	5.0	109.32	81.21
5	200	5.0	109.32	81.21
6	50	7.0	10.02	162.42
7	1300	7.0	104.37	162.42

The technical route of this study can be referred to Figure 6.

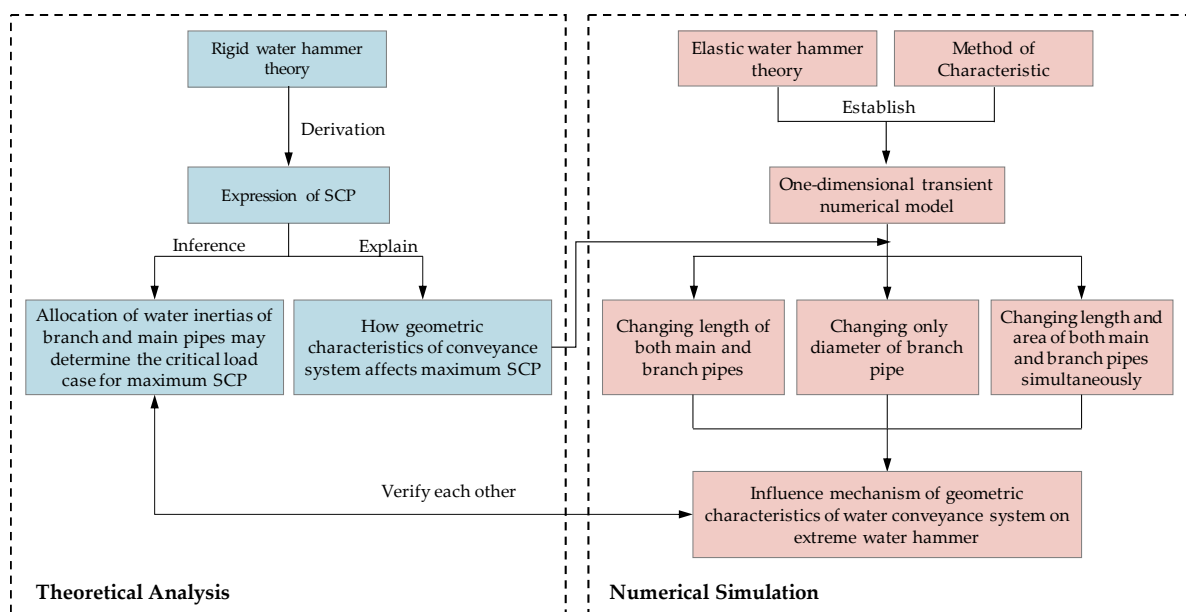


Figure 6. Flowchart of the technical route.

3. Numerical Simulation and Results

To further validate the above conclusions, a numerical simulation was conducted herein. The numerical simulation for the influence of the geometric characteristics of the upstream pipelines on the maximum SCP can be carried out through following three scenarios. Scenario 1, keeping the

total length of the upstream pipelines to be constant, and allocating the main pipe length and branch pipe length. Scenario 2, only altering the branch pipe area, and the rest of the parameters are kept unchanged. Scenario 3, changing the length and area of both main and branch pipes simultaneously to keep $T_{w,u}$ of each scheme the same as the original one. For convenient analysis, define $\eta_1 = T_{wb,u}/T_{w,u}$, characterizing the proportion of the water inertia of the branch pipe to that of the upstream pipelines.

The procedure of the TLR is described as follows. RPT 1 rejects full load at $t = 0$ as the first load rejection turbine, and after some interval of time, RPT 2 rejects full load caused by violent hydraulic disturbance as the subsequent load rejection turbine. The worst interval time for extreme high SCP can be obtained by repeated trial calculation.

3.1. Scenario 1: Changing Length of Both Main and Branch Pipes

For Scenario 1, the total length of the diversion pipelines was kept at a constant of 1320 m, and diameters of the main and branch pipes remained at 6.8 m and 2.8 m, respectively. The downstream water conveyance system was consistent with Table 1. The other parameters of different schemes are shown in Table 2, as well as the results of the maximum SCP.

Table 2. Conduits parameters and corresponding results for Scenario 1.

Main Pipe	L_1 (m)	934.26	997.58	1096.45	1200.00	1271.63
	D_1 (m)			6.8		
	f_1 (m ²)			36.32		
	$T_{wm,u}$ (s)	0.57	0.61	0.67	0.73	0.77
Branch Pipe	L_3 (m)	385.74	322.42	223.55	120.00	48.37
	D_3 (m)			2.8		
	f_3 (m ²)			6.16		
	$T_{wb,u}$ (s)	1.38	1.16	0.80	0.43	0.17
$T_{w,u}$ (s)		1.95	1.77	1.47	1.16	0.94
η_1		0.71	0.66	0.55	0.37	0.18
Max. SCP during SLR (m)		651.17	645.25	637.63	628.02	622.28
Max. SCP during TLR (m)		673.10	666.61	652.35	634.03	622.28
Worst Interval Time (s)		4.8	4.8	4.8	1.8	0 ¹

¹ SLR actually is the special case of TLR. If the maximum spiral case pressure (SCP) of TLR is always equal or less than that of SLR, the worst interval time is 0 s.

As shown in Table 2, on the premise of constant total length, main pipe areas, and branch pipe areas, the water inertia time constant of the main pipe ($T_{wm,u}$) increased with the increasing main pipe length. While the decreasing branch pipe length led to the decrease in $T_{wb,u}$. Eventually, the ratio of the water inertia of the branch pipe to that of the upstream pipelines (η_1) decreased. The results illustrate that the maximum SCP decreased with decreasing η_1 , which is consistent with conventional theory. The difference is that at the larger ratio of η_1 ($\eta_1 \geq 0.37$), the maximum SCP occurred in TLR rather than SLR. Figure 7 gives the maximum SCP with different time intervals for each η_1 in Scenario 1. For the four schemes of $\eta_1 = 0.71$, $\eta_1 = 0.66$, $\eta_1 = 0.55$, and $\eta_1 = 0.37$, the worst interval time was 4.8 s, 4.8 s, 4.8 s, and 1.8 s, respectively. The maximum SCPs increased with increasing time intervals and attained peak value of 673.10 m, 666.61 m, 652.35 m, and 634.03 m at corresponding worst interval times. The variation of the SCP at worst interval time for different η_1 can be referred to Figure 8. In particular, the difference between maximum SCP during SLR and TLR at 4.8 s reached 21.9 m for $\eta_1 = 0.71$. If the safety margin is not reserved enough, the unavoidable extreme pressure increase during TLR may cause the rupture of spiral case, which will lead to serious damage to the system. As for $\eta_1 = 0.18$, with the increase of time intervals, the maximum SCP presented a downward trend. That is, the maximum SCP appeared during SLR. The unexpected phenomenon herein is different from the conventional theory that maximum SCP occurs in SLR, but greatly related to the water inertia of both main and branch pipes.

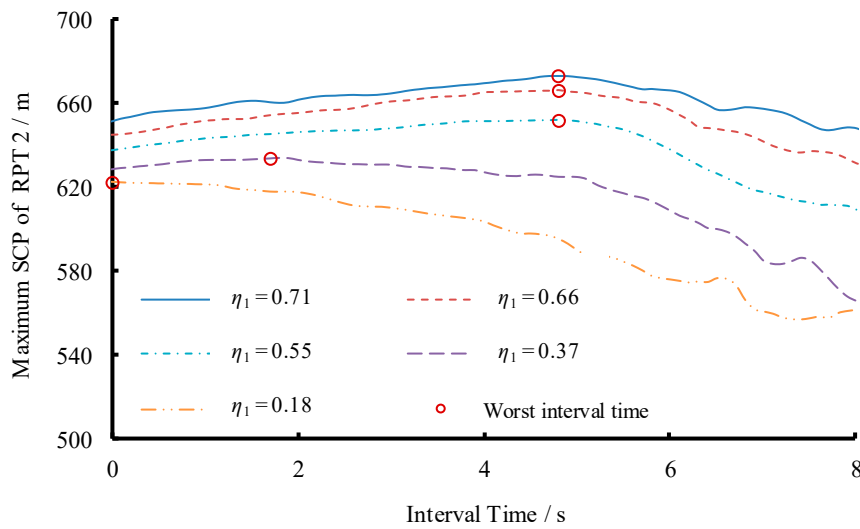


Figure 7. Maximum SCP with different time intervals of different η_1 for Scenario 1.

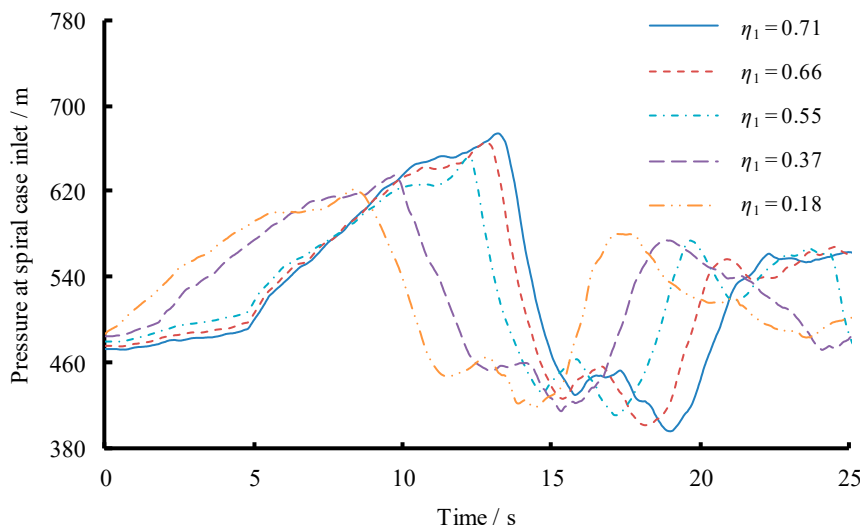


Figure 8. Spiral case pressure of different η_1 versus time for Scenario 1.

Taking the typical schemes of $\eta_1 = 0.71$ and $\eta_1 = 0.18$ for further investigation as they presented the different results. Figures 8 and 9 give the time history of discharge of the main and branch pipes during SLR and TLR for $\eta_1 = 0.71$ and $\eta_1 = 0.18$, respectively. The total closure time for SLR was 26 s, while it was $(26 + t_c)$ s for TSL. That is, TLR actually extended the total closure time of the system compared with SLR, which was consistent with analysis in Section 2. The flow gradient in the main pipe was definitely decreased under TLR compared with SLR. Besides, $\frac{dQ_T}{dt}$ was negative before the discharge first drops to the valley. Thus $-\frac{dQ_T}{dt}\Big|_{TLR} + \frac{dQ_T}{dt}\Big|_{SLR} < 0$ is always valid. The change rate of discharge of main and branch pipes at the instant for maximum SCP are listed in Table 3, and can be seen in Figures 9 and 10 as well. For $\eta_1 = 0.71$, $\left(-\frac{dQ_T}{dt}\Big|_{TLR} + \frac{dQ_T}{dt}\Big|_{SLR}\right) = 16.16 - 27.75 = -11.59 \text{ m}^2/\text{s}^2 < 0$, while for $\eta_1 = 0.18$, $\left(-\frac{dQ_T}{dt}\Big|_{TLR} + \frac{dQ_T}{dt}\Big|_{SLR}\right) = 22.4 - 32.27 = -9.87 \text{ m}^2/\text{s}^2 < 0$.

The smaller the water inertia in main pipe, the severer change in flow gradient between TLR and SLR. When SLR occurred, the discharge of RPT 2 dropped to the first valley at a greater rate of discharge change in a shorter time for the worst time interval. The flow gradient of the branch pipe of RPT 2 was much greater than SLR. Thus $-\frac{dQ_2}{dt}\Big|_{TLR} + \frac{dQ_2}{dt}\Big|_{SLR} > 0$ is always valid. Similarly, for $\eta_1 = 0.71$, there

exists $\left(-\frac{dQ_2}{dt}\Big|_{TLR} + \frac{dQ_2}{dt}\Big|_{SLR}\right) = 20.08 - 13.66 = 6.42 \text{ m}^2/\text{s}^2 > 0$, while for $\eta_1 = 0.18$, $\left(-\frac{dQ_2}{dt}\Big|_{TLR} + \frac{dQ_2}{dt}\Big|_{SLR}\right) = 45.69 - 20.71 = 24.98 \text{ m}^2/\text{s}^2 > 0$. The smaller the water inertia in branch pipe, the severer change in flow gradient between TLR and SLR. The results are consistent with the theoretical analysis.

According to Equation (11) or Equation (14),

$$\begin{aligned} (h_{tu2 \text{ TLR}} - h_{tu2 \text{ SLR}})_{\eta_1=0.71} &= T_{wm,u} \left(-\frac{dq_T}{dt}\Big|_{TLR} + \frac{dq_T}{dt}\Big|_{SLR}\right) + T_{wb,u} \left(-\frac{dq_2}{dt}\Big|_{TLR} + \frac{dq_2}{dt}\Big|_{SLR}\right) \\ &= 0.57 \times (-0.134) + 1.38 \times 0.074 = 0.026 > 0 \end{aligned} \quad (22)$$

Equations (22) and (23) and Table 3 indicate the critical load case for maximum SCP was closed related to the water inertia of the branch and main pipes, which was determined by the geometric dimension of the upstream water conveyance system. The maximum SCP occurred in TLR for larger η_1 (≥ 0.37), while it came to SLR for smaller η_1 (≤ 0.18). Additionally, the worst interval times, changing from 4.8 s to 1.8 s and finally 0 s, also explain the effect of the different η_1 on the SCP. In conclusion, the allocation of the water inertia in main and branch pipes was the critical factor determining in which load cases the maximum SCP will occur. When η_1 is at a large value, the water inertia in branch pipe is the dominant effect for inducing maximum SCP during TLR. If the water inertia in the main pipe becomes the dominant factor ($\eta_1 \leq 0.18$), maximum SCP will occur in SLR condition.

Additionally, Figures 11 and 12 present the time histories of the discharge of the main pipe and branch pipe for different η_1 , respectively. For the schemes of $\eta_1 = 0.71$, $\eta_1 = 0.66$ and $\eta_1 = 0.55$, the worst interval times were all 4.8 s. The discharge variation curve clusters of the main pipe for these three schemes had almost the same variation trend before the instant for maximum SCP. However, obvious differences appeared for the branch pipe discharge curve clusters after the load rejection of RPT 2, which indicates that the geometric dimension change of the branch pipe has greater influence on the maximum SCP.

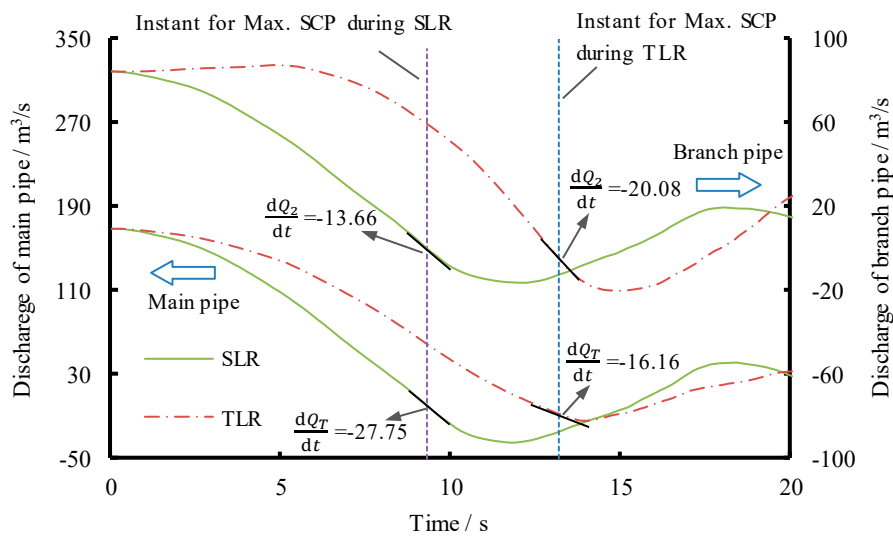


Figure 9. Discharge of the main and branch pipes versus time during SLR and TLR for $\eta_1 = 0.71$.

Table 3. Change rate of discharge of main and branch pipes at the instant for maximum spiral case pressure (SCP).

η_1	Load Cases	Instant for Maximum SCP (s)	dQ_T/dt (m^3/s^2)	dQ_2/dt (m^3/s^2)	$h_{tu2 \text{ TLR}} - h_{tu2 \text{ SLR}}$	Critical Load Case
0.71	SLR	9.3	-27.75	-13.66	>0	TLR
	TLR	13.2	-16.16	-20.08		
0.18	SLR	8.3	-32.27	-20.71	<0	SLR
	TLR	10.9	-22.4	-45.69		

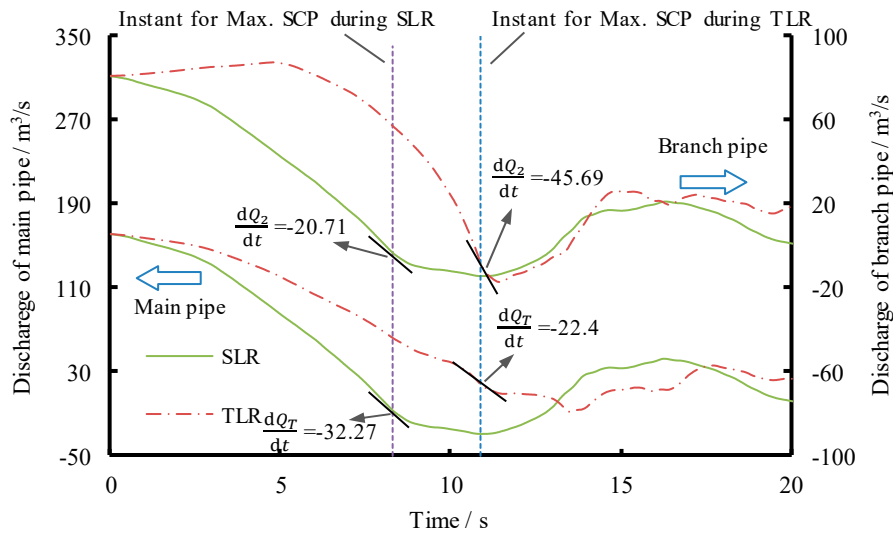


Figure 10. Discharge of the main and branch pipes versus time during SLR and TLR for $\eta_1 = 0.18$.

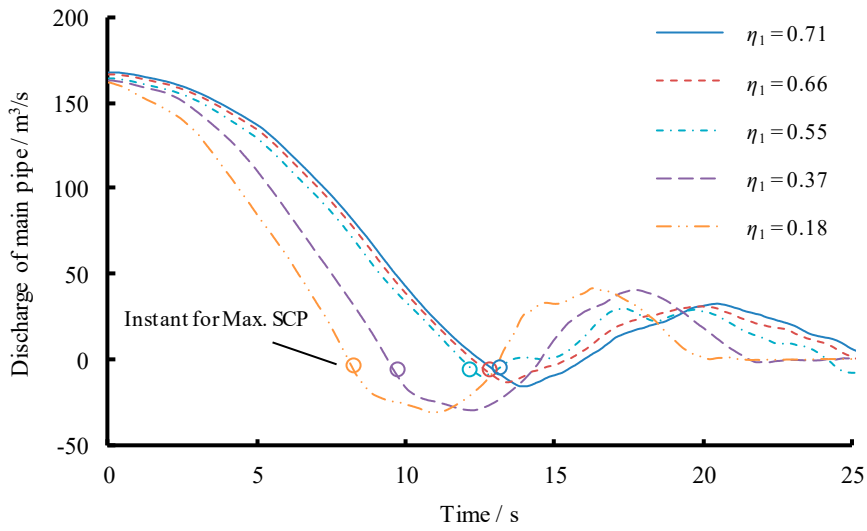


Figure 11. Main pipe discharge of different η_1 versus time for Scenario 1.

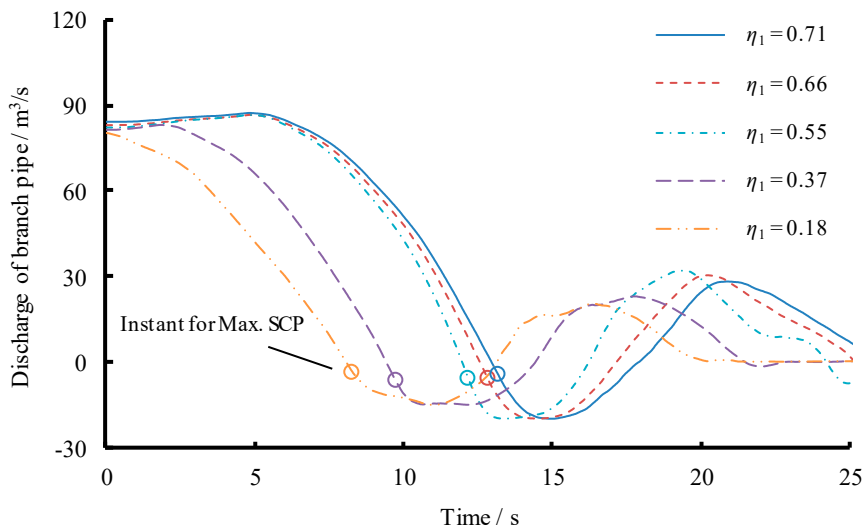


Figure 12. Branch pipe discharge of different η_1 versus time for Scenario 1.

3.2. Scenario 2: Changing Diameter of Branch Pipe

Since the change of the branch pipe diameter can greatly influence proportion of the water inertia of the branch pipe to that of the upstream pipelines, herein only the diameter of the branch pipe is changed for Scenario 2. The rest parameters are kept constant, as well as the downstream water conveyance system. The other parameters of different schemes and results are listed in Table 4.

Table 4. Conduits parameters and corresponding results for Scenario 2.

Main Pipe	L_1 (m)	1200				
	D_1 (m)	6.8				
	f_1 (m ²)	36.32				
	$T_{wm,u}$ (s)	0.73				
Branch Pipe	L_3 (m)	120.00				
	D_3 (m)	5.02	4.59	3.82	2.8	1.78
	f_3 (m ²)	19.79	16.54	11.47	6.16	2.48
	$T_{wb,u}$ (s)	0.13	0.16	0.23	0.43	1.07
$T_{w,u}$ (s)	0.86	0.89	0.96	1.16	1.80	
η_1	0.16	0.18	0.24	0.37	0.59	
Max. SCP during SLR (m)	616.88	618.02	621.17	628.02	646.92	
Max. SCP during TLR (m)	616.88	618.02	621.83	634.03	661.66	
Worst Interval Time (s)	0	0	0.6	1.8	4.8	

As shown in Table 4 and Figures 13 and 14, the results present the same law to that of Scenario 1. With the decrease of the branch pipe diameter, the water inertia of the upstream pipelines increased, thereby increasing the maximum SCP. For the schemes of $\eta_1 = 0.16$ and $\eta_1 = 0.18$, the maximum SCP both appeared in LSR because of the relative low proportion of water inertia in the branch pipe. When η_1 rose to 0.24, the maximum SCP began to appear in TLR. At this point, the worst interval time was 0.6 s, and the difference in the maximum SCP between TLR and SLR was merely 0.66 m. After that, the maximum SCP still occurred in TLR and the difference in the maximum SCP between TLR and SLR was increasing with the increasing η_1 , as well as the worst interval time. The results of Scenario 2 also indicate that the allocation change of the water inertia between the main and branch pipes may result in the critical load case transfer for maximum SCP. Figures 15 and 16 give the discharge variations of main and branch pipes of different η_1 for Scenario 2. The diameter changes in the branch pipe also influence the discharge variation of both main and branch pipes.

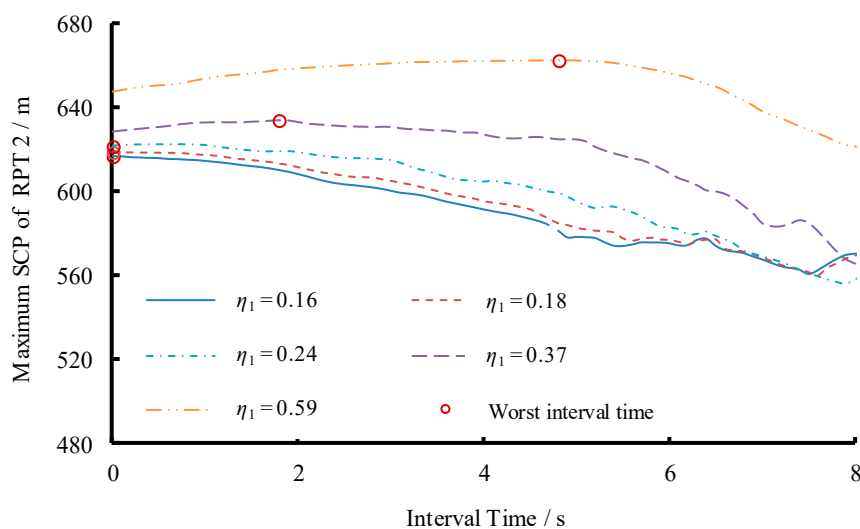


Figure 13. Maximum SCP with different time intervals of different η_1 for Scenario 2.

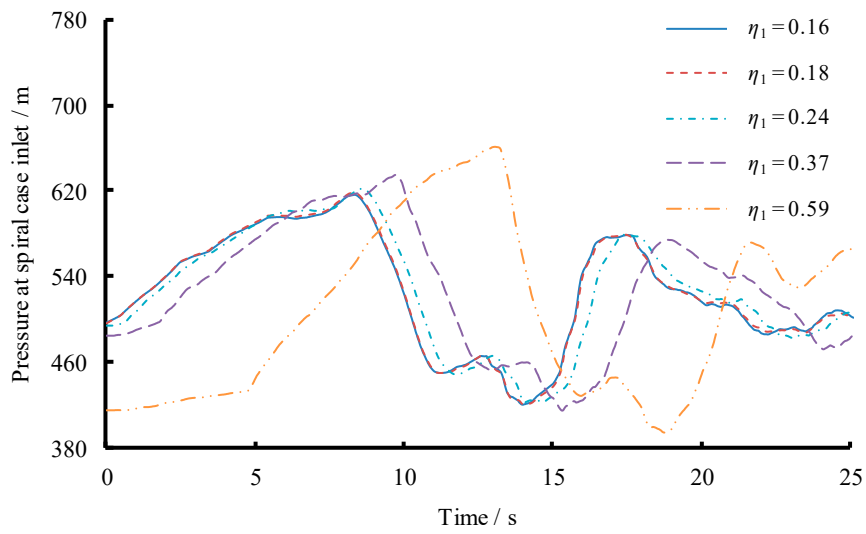


Figure 14. Spiral case pressure of different η_1 versus time for Scenario 2.

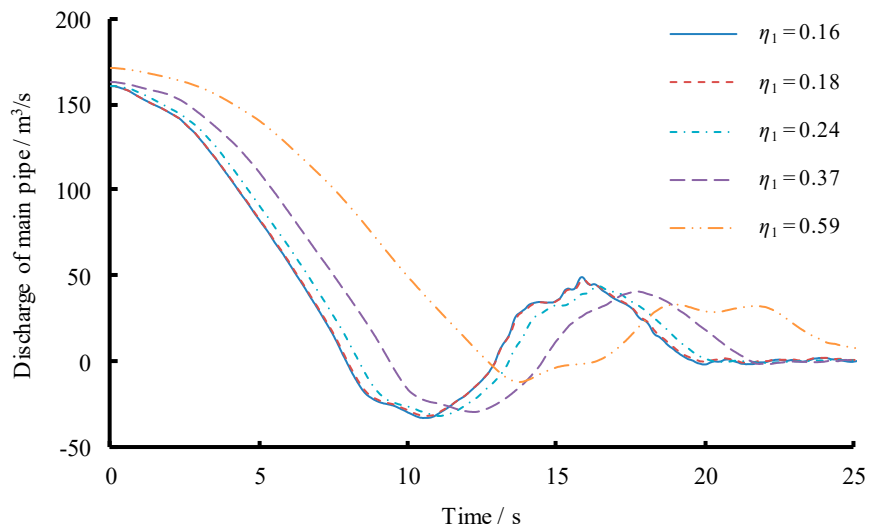


Figure 15. Main pipe discharge of different η_1 versus time for Scenario 2.

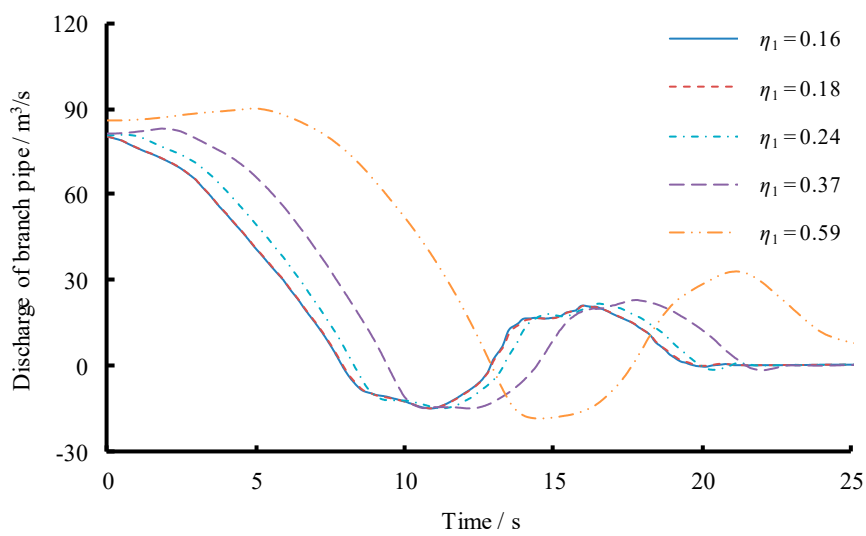


Figure 16. Branch pipe discharge of different η_1 versus time for Scenario 2.

3.3. Scenario 3: Changing Length and Area of Both Main and Branch Pipes Simultaneously

To further reveal the effect of water inertia on extreme water hammer, the water inertia time constant of both branch and main pipe were kept constant in Scenario 3. The length and area of both main and branch pipes were simultaneously changed to keep $T_{wm,u}$ and $T_{wb,u}$ of each scheme the same as the original one. The rest of the parameters were kept constant, as well as the downstream water conveyance system. Table 5 lists the other parameters of different schemes and corresponding results.

Table 5. Conduits parameters and corresponding results for Scenario 3.

Main Pipe.	L_1 (m)	934.26	997.58	1096.45	1200.00	1271.63
	D_1 (m)	6.0	6.2	6.5	6.8	7.0
	f_1 (m ²)	28.27	30.19	33.18	36.32	38.48
	$T_{wm,u}$ (s)			0.73		
Branch Pipe	L_3 (m)	385.74	322.42	223.55	120.00	48.37
	D_3 (m)	5.02	4.59	3.82	2.8	1.78
	f_3 (m ²)	19.79	16.54	11.47	6.16	2.48
	$T_{wb,u}$ (s)			0.43		
$T_{w,u}$ (s)				1.16		
η_1				0.37		
Max. SCP during SLR (m)		627.46	627.51	627.65	628.02	628.04
Max. SCP during TLR (m)		633.55	633.76	634.10	634.03	633.94
Worst Interval Time (s)		1.9	1.9	1.9	1.8	1.9

For the five schemes in Scenario 3, the values of $T_{wm,u}$ and $T_{wb,u}$ were kept constant as 0.73 and 0.43, respectively, by changing the lengths and areas of the main and branch pipes simultaneously. Thereby $\eta_1 = 0.37$ remained unchanged. As shown in Table 5, the maximum SCP of each scheme was almost the same no matter if it was the SLR or TLR. The maximum difference between the five schemes was within 0.6 m. Figure 17 presents the maximum SCP with different time intervals for each scheme of Scenario 3, which had almost the same variation trend. Additionally, the worst interval time for each scheme under TLR was about 1.9 s, and also can be regarded to be the same. As for the SCP for each scheme of Scenario 3, although the initial pressure was not the same due to the different head loss, nearly the same extreme SCP was reached, meaning the curves varied in the same way (seen in Figure 18). Moreover, the discharge variation curve clusters of the main and branch pipes are almost overlapped, which is shown in Figure 19. The above results verify the conclusion that the discharge change rate remained little changed, thereby the extreme SCPs were almost the same providing the water inertia time constants of both main and branch pipelines were kept constant. It should be noted that the slight difference in discharge was due to the influence of head loss. Although η_1 is kept constant for each scheme, there is no guarantee that head loss is the same. Except from this factor, the difference of pressure change curve clusters was also related to the influence of the velocity head.

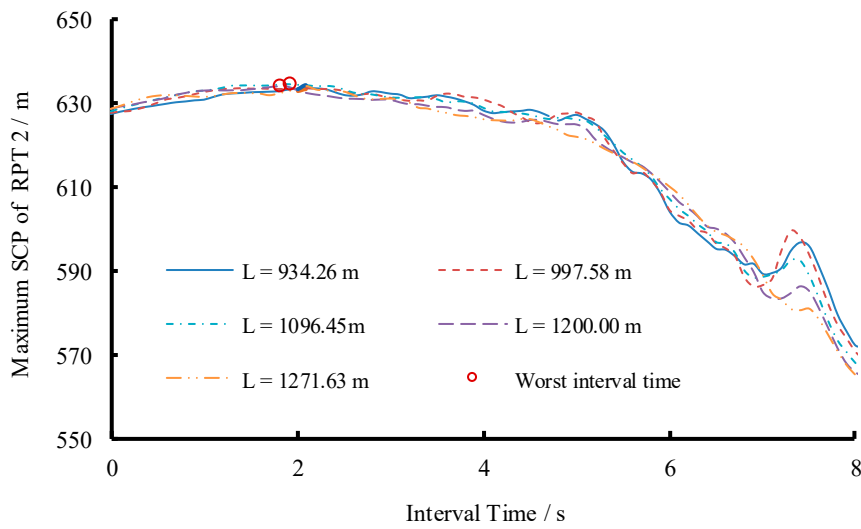


Figure 17. Maximum SCP with different time intervals for each scheme of Scenario 3.

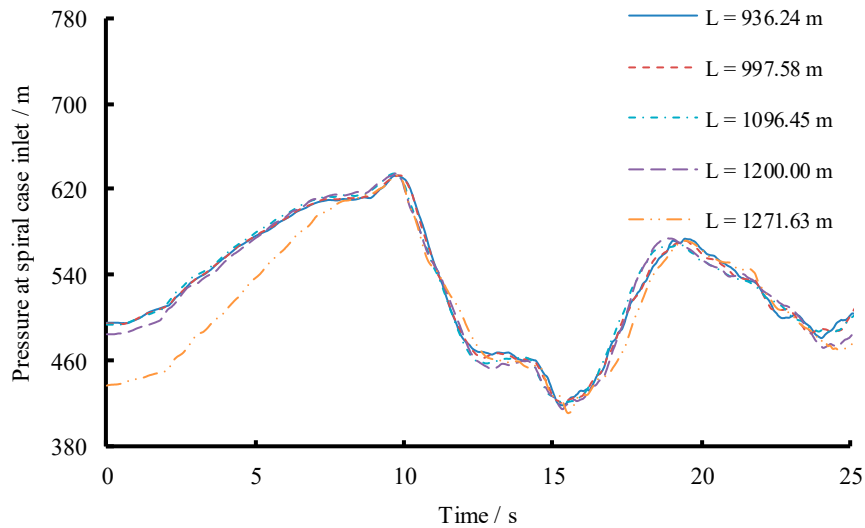


Figure 18. Maximum SCP with different time intervals for each scheme of Scenario 3.

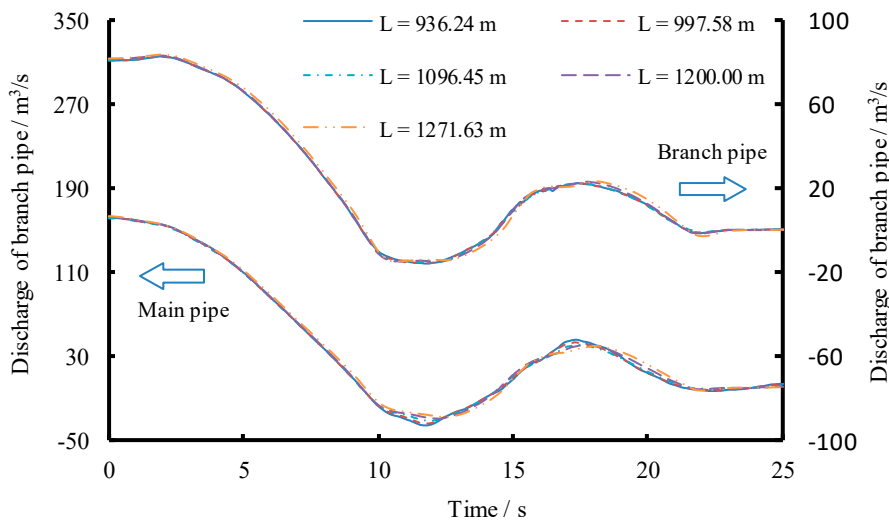


Figure 19. Main and branch pipe discharge versus time for each scheme of Scenario 3 during TLR.

4. Discussion

For conventional hydroelectrical power plants, SLT is generally accepted as the critical load case for extreme water hammer. However, it is not completely applied for the PSPs because of the unique S-shaped characteristics. The above theoretical analysis and numerical simulation show that the maximum SCP during load rejection is closely related to the geometric dimensions of the upstream water diversion system, including the area and length of both branch and main pipes. The changes of the geometric characteristics of the upstream pipelines actually cause the changes in the water inertia. When the water inertia time constant in the branch pipe is dominant, the extreme water hammer will occur under TLR condition. For the numerical simulation herein, if $\eta_1 > 0.24$ (η_1 denotes the ratio of the water inertia of the branch pipe to that of the upstream pipelines), then the maximum SCP would appear in TLR rather than SLR (as shown in Figure 20), which is not consistent with the conventional knowledge. Moreover, with the continuous increase of η_1 , the differences of the maximum SCP between SLR and TLR increased greatly. Especially, for $\eta_1 = 0.71$, the maximum SCP during TLR was nearly 22 m greater than that during SLR, which is inconceivable and catastrophic for the PSP system. Therefore, in the design stage of a PSP, the importance of this phenomenon should be fully recognized, and the geometric characteristics of branch pipes should be carefully examined to obtain a reasonable and relatively small η_1 , so as to ensure the maximum SCP occurring at the load case of SLR.

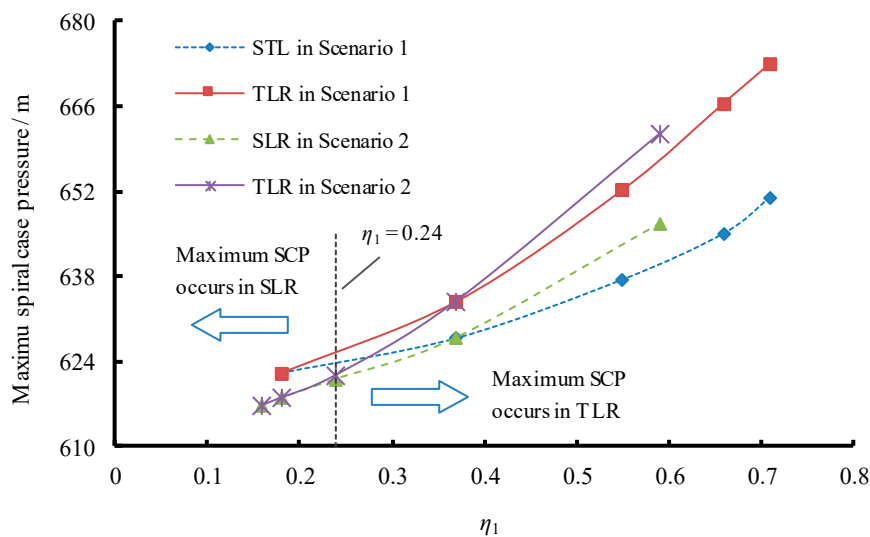


Figure 20. Variation of maximum SCP with η_1 .

In addition, if the pipeline area and length are changed at the same time to keep constant of η_1 , the maximum SCP is almost the same, verifying the inference from theoretical analysis. The achievements also provide another idea on the optimal design of the water conveyance system of the PSP.

5. Conclusions

The maximum SCP is one of the control parameters for the water conveyance system design of a PSP. As a result, the determination of the critical load case becomes the primary task. In this study, the effect of geometric characteristics of upstream pipelines on extreme water hammer during load rejection was examined. Rigid water hammer theory was introduced for quantitative analysis. Based on MOC and modified Suter transformations, the dynamic transient numerical model was developed and applied to a practical engineering of a numerical simulation. The fact that TLR can be the critical load case for maximum SCP is presented, and the influence mechanism of the geometric dimension on the maximum SCP was revealed.

In conclusion, the extreme water hammer pressure is closely related to geometric characteristics of the water conveyance system, namely the allocation of the water inertia time constant of the main and branch pipelines. If the water inertia in the branch pipeline is dominant, the maximum SCP will occur under TLR condition, and vice versa. The ratio of the water inertia of the branch pipe to that of the upstream pipelines η_1 can serve as the index to measure whether the maximum SCP is occurring in SLR or TLR. With the increase of η_1 , the differences of the maximum SCP between SLR and TLR increase greatly. Moreover, the discharge change rate remains little changed, providing the water inertia time constants of both main and branch pipelines are kept constant (a constant of η_1), eventually resulting in the unchanged maximum SCP.

Author Contributions: Conceptualization, S.C., J.Z., and X.Y.; methodology, S.C. and G.L.; validation, J.Z.; writing—original draft, S.C.; writing—review and editing, G.L. and X.Y.

Funding: This research was supported by the National Natural Science Foundation of China (Grant No. 51709087 and No. 51839008), and the Fundamental Research Funds for the Central Universities (Grant No. 2018B55514).

Conflicts of Interest: The authors declare no conflict of interest.

Nomenclature

c	Constant selected between 1 and 1.5	-
D	Diameter of runner	m
f_i	Cross-sectional area of i -th pipeline	m ²
f_{sc}	Area at spiral case end	m ²
f_{dt}	Area at draft tube inlet	m ²
g	Gravitational acceleration	m/s ²
H	Working head of RPT	m
H_{Fu}	Piezometric head at upstream bifurcation	m
H_r	Rated head	m
h	Dimensionless head	-
h_{tu}	Dimensionless head at spiral case end	-
H_{tu1}	Piezometric head at the spiral case of RPT 1	m
H_{tu2}	Piezometric head at the spiral case of RPT 2	m
i	Number of pipeline reaches, =1–3	-
I	Inertia polar moment	kg·m ²
L_i	Length of i -th pipeline reach	m
M	Shaft torque	N·m
M_r	Rated shaft torque	N·m
M_{11}	Unit torque	N·m
N	Rotational speed	r/min
N_r	Rated rotational speed	r/min
n	Dimensionless rotational speed	r/min
n_0	Result of a previous time step of n	r/min
n_{11}	Unit speed	r/min
n_{11r}	Rated unit speed	r/min
P	Power generated by RPT	kW
P_g	Power absorbed by generator	kW
Q	Demand discharge of RPT	m ³ /s
q	Dimensionless discharge	-
q_1	Dimensionless demand discharge of RPT 1	-
Q_1	Demand discharge of RPT 1	m ³ /s
Q_{11}	Unit discharge	m ³ /s
Q_{11r}	Rated unit discharge	m ³ /s
q_2	Dimensionless demand discharge of RPT 2	-
Q_2	Demand discharge of RPT 2	m ³ /s
Q_r	Rated discharge	m ³ /s
q_T	Dimensionless rated discharge	-

Q_T	Discharge of headrace tunnel	m^3/s
R_g	Gyration radius	m
t	Time	s
t_c	Worst interval time	s
T_a	Mechanical starting time	s
$T_{w,u}$	Water inertia time constant of upstream pipelines	s
$T_{wm,u}$	Water inertia time constant of upstream main pipe	s
$T_{wb,u}$	Water inertia time constant of upstream branch pipe	s
W	Weight	kg
WB	Turbine torque characteristics	-
WH	Turbine head characteristics	-
x	Polar angle	rad
y	Dimensionless guide vane opening	-
z	Dimensionless water level	-
z_u	Dimensionless upstream reservoir water level	-
Z_u	Upstream reservoir water level	M
α_i	Head loss coefficient of i -th pipeline reach	-
α_0	Wicket gate opening	$^\circ$
β	Dimensionless torque	-
β_0	Result of a previous time step of β	-
ω	Angular velocity	rad/s
η_1	Proportion of water inertia of branch pipe to that of upstream pipelines	-
Δt	Time step	s
$\frac{dq_1}{dt}$	Dimensionless rate of discharge change of RPT 1	s^{-1}
$\frac{dq_2}{dt}$	Dimensionless rate of discharge change of RPT 2	s^{-1}
$\frac{dq_T}{dt}$	Dimensionless rate of discharge change of headrace tunnel	s^{-1}
$\frac{dQ_1}{dt}$	Rate of discharge change of RPT 1	s^{-1}
$\frac{dQ_2}{dt}$	Rate of discharge change of RPT 2	s^{-1}
$\frac{dQ_T}{dt}$	Rate of discharge change of headrace tunnel	s^{-1}

Abbreviations

DTP	Draft tube pressure
MOC	Method of characteristic
PSP	Pumped storage plant
RES	Renewable energy sources
RPT	Reversible pump turbine
SCP	Spiral case pressure
SLR	Simultaneous load rejection
TLR	Two-stage load rejection

References

1. Dai, H.C.; Xie, X.X.; Xie, Y.; Liu, J.; Masui, T. Green growth: The economic impacts of large-scale renewable energy development in China. *Appl. Energy* **2016**, *162*, 435–449. [[CrossRef](#)]
2. Ellabban, O.; Abu-Rub, H.; Blaabjerg, F. Renewable energy resources: Current status, future prospects and their enabling technology. *Renew. Sustain. Energy Rev.* **2014**, *39*, 748–764. [[CrossRef](#)]
3. Bhattacharya, M.; Paramati, S.R.; Ozturk, I.; Bhattacharya, S. The effect of renewable energy consumption on economic growth: Evidence from top 38 countries. *Appl. Energy* **2016**, *162*, 733–741. [[CrossRef](#)]
4. Rehman, S.; Al-Hadhrani, L.M.; Alam, M.M. Pumped hydro energy storage system: A technological review. *Renew. Sustain. Energy Rev.* **2015**, *44*, 586–598. [[CrossRef](#)]
5. Zeng, W.; Yang, J.D.; Yang, W.J. Instability analysis of pumped-storage stations under no-load conditions using a parameter-varying model. *Renew. Energy* **2016**, *90*, 420–429. [[CrossRef](#)]

6. Chaudhary, P.; Rizwan, M. Energy management supporting high penetration of solar photovoltaic generation for smart grid using solar forecasts and pumped hydro storage system. *Renew. Energy* **2018**, *118*, 928–946. [[CrossRef](#)]
7. Ghasemi, A.; Enayatzare, M. Optimal energy management of a renewable-based isolated microgrid with pumped-storage unit and demand response. *Renew. Energy* **2018**, *123*, 460–474. [[CrossRef](#)]
8. Zeng, M.; Feng, J.J.; Xue, S.; Wang, Z.J.; Zhu, X.L.; Wang, Y.J. Development of China's pumped storage plant and related policy analysis. *Energy Policy* **2013**, *61*, 104–113. [[CrossRef](#)]
9. Hino, T.; Lejeune, A. Pumped storage hydropower developments. *Compre. Renew. Energy* **2012**, *6*, 405–434. [[CrossRef](#)]
10. Allievi, L. *Teoria del Colpo D'ariete*; Stabilimenti grafici Stucchi: Milan, Italy, 1913.
11. Wood, F.M. The Application of heaviside's Operational Calculus to the Solution of Problems in Waterhammer. *Trans. ASME* **1937**, *59*, 707–713.
12. Rich, G. Waterhammer Analysis by the Laplace-Mellin Transformations. *Trans. ASME* **1945**, *59*, 361–376.
13. Parmakian, J. *Water-Hammer Analysis*; Prentice-Hall, Inc.: Englewood Cliffs, NJ, USA, 1955.
14. Streeter, V.L.; Lai, C. Waterhammer Analysis Including Fluid Friction. *Trans. Am. Soc. Civ. Eng.* **1963**, *128*, 1491–1524. [[CrossRef](#)]
15. Streeter, V.L.; Wylie, E.B. *Hydraulic Transients*; McGraw-Hill: New York, NY, USA, 1967.
16. Chaudhry, M.H. *Applied Hydraulic Transients*; Van Nostrand Reinhold: New York, NY, USA, 1987.
17. Wylie, E.B.; Streeter, V.L.; Suo, L.S. *Fluid Transients in Systems*; Prentice-Hall, Inc.: Englewood Cliffs, NJ, USA, 1993.
18. Wood, D.J.; Dorsch, R.G.; Lightnor, C. Wave-Plan Analysis of Unsteady Flow in Closed Conduits. *J. Hydraul. Div.* **1966**, *92*, 83–110.
19. Guinot, V. Riemann Solvers for Water Hammer Simulations by Godunov Method. *Int. J. Numer. Methods Eng.* **2002**, *49*, 851–870. [[CrossRef](#)]
20. Izquierdo, J.; Iglesias, P.L. Mathematical modelling of hydraulic transients in simple systems. *Math. Comput. Model.* **2002**, *35*, 801–812. [[CrossRef](#)]
21. Yang, W.J.; Yang, J.D.; Guo, W.C.; Zeng, W.; Wang, C.; Saarinen, L.; Norrlund, P. A Mathematical Model and Its Application for Hydro Power Units under Different Operating Conditions. *Energies* **2015**, *8*, 10260–10275. [[CrossRef](#)]
22. Rezaghi, A.; Riasi, A. Sensitivity analysis of transient flow of two parallel pump-turbines operating at runaway. *Renew. Energy* **2016**, *86*, 611–622. [[CrossRef](#)]
23. Rezaghi, A.; Riasi, A. The interaction effect of hydraulic transient conditions of two parallel pump-turbine units in a pumped-storage power plant with considering "S-shaped" instability region: Numerical simulation. *Renew. Energy* **2018**, *118*, 896–908. [[CrossRef](#)]
24. Hu, J.H.; Yang, J.D.; Zeng, W.; Yang, J.B. Transient Pressure Analysis of a Prototype Pump Turbine: Field Tests and Simulation. *J. Fluids Eng.* **2018**, *140*, 071102. [[CrossRef](#)]
25. Zhou, D.Q.; Chen, H.X.; Zhang, L.G. Investigation of Pumped Storage Hydropower Power-Off Transient Process Using 3D Numerical Simulation Based on SP-VOF Hybrid Model. *Energies* **2018**, *11*, 1020. [[CrossRef](#)]
26. Fu, X.; Li, D.; Wang, H.; Zhang, G.; Li, Z.; Wei, X. Analysis of transient flow in a pump-turbine during the load rejection process. *J. Mech. Sci. Technol.* **2018**, *32*, 2069–2078. [[CrossRef](#)]
27. Fu, X.; Li, D.; Wang, H.; Zhang, G.; Li, Z.; Wei, X.; Qin, D. Energy analysis in a pump-turbine during the load rejection process. *J. Fluids Eng.* **2018**, *140*, 101107. [[CrossRef](#)]
28. Kuwabara, T.; Katayama, K.; Nakagawa, H.; Hagiwara, H. Improvements of transient performance of pump turbine upon load rejection. In Proceedings of the IEEE Power Engineering Society Summer Meeting, Seattle, WA, USA, 16–20 July 2000; pp. 1783–1788. [[CrossRef](#)]
29. Yu, X.; Zhang, J.; Miao, D. Innovative closure law for pump-turbines and field test verification. *J. Hydraul. Eng.* **2015**, *141*, 05014010. [[CrossRef](#)]
30. Li, X.Q.; Tang, X.L.; Shi, X.Y.; Chen, H.H.; Li, C.S. Load rejection transient with joint closing law of ball-valve and guide vane for two units in pumped storage power station. *J. Hydroinform.* **2018**, *20*, 301–315. [[CrossRef](#)]
31. Zhang, J.; Wang, D.L.; Hu, J.Y.; Zhou, J.; Fang, J. Study on Field Test and Simulating Calculation Following Load Rejections of Tongbai Pumped Storage Power Station. In Proceedings of the 2009 ASME Fluids Engineering Division Summer Conference, Jacksonville, FL, USA, 10–14 August 2008.

32. Chen, S.; Zhang, J.; Li, G.H.; Yu, X.D. Load rejection test and numerical prediction of critical load case scenarios for pumped storage plant. In Proceedings of the ASME 2017 Fluids Engineering Division Summer Meeting, FEDSM 2017, Waikoloa, HI, USA, 30 July–3 August 2017.
33. Yin, J.L.; Wang, D.Z.; Wei, X.Z.; Wang, L.Q. Hydraulic Improvement to Eliminate S-Shaped Curve in Pump Turbine. *ASME. J. Fluids Eng.* **2013**, *135*, 071105. [[CrossRef](#)]
34. Yokoyama, T.; Shimmei, K. Dynamic Characteristics of Reversible Pump Turbines in Pumped Storage Plants. In Proceedings of the USDE and EPRI Symposium, Boston, MA, USA, 24–26 August 1984.
35. Chen, S.; Zhang, J.; Wang, X.C. Characterization of surge superposition following 2-stage load rejection in hydroelectric power plant. *Can. J. Civil Eng.* **2016**, *43*, 844–850. [[CrossRef](#)]
36. Zhang, J.; Suo, L.S. Study on tailrace surge chamber installation and hydraulic transients at pumped-storage plant. *Water Res. Power* **2008**, *26*, 83–87.
37. Zhang, J.; Lu, W.H.; Hu, J.Y.; Fan, B.Q. Study on the hydraulic transients of pumped-turbines load successive rejection in pumped storage plant. In Proceedings of the 5th Joint ASME/SME Fluids Engineering Summer Conference, FEDSM 2007, San Diego, CA, USA, 30 July–2 August 2007; pp. 57–61. [[CrossRef](#)]
38. Zhang, J.; Lu, W.H.; Fan, B.Q.; Hu, J.Y. The influence of layout of water conveyance system on the hydraulic transients of pump-turbines load successive rejection in pumped storage station. *J. Hydroelectric Eng.* **2008**, *27*, 158–162.
39. Zeng, W.; Yang, J.D. Effects of pipe diameters on the pressures during delayed load rejection in high-head pumped storage power stations. In Proceedings of the 27th IAHR Symposium on Hydraulic Machinery and System, Montreal, QC, Canada, 22–26 September 2014.
40. Zeng, W.; Yang, J.D.; Hu, J.H.; Yang, J.B. Guide-vane closing schemes for pump-turbines based on transient characteristics in S-shaped region. *ASME. J. Fluids Eng.* **2016**, *138*, 051302. [[CrossRef](#)]
41. Zeng, W.; Yang, J.D.; Tang, R.B.; Yang, W.J. Extreme water-hammer pressure during one-after-another load shedding in high-head pumped-storage stations. *Renew. Energy* **2016**, *99*, 35–44. [[CrossRef](#)]
42. Fang, Y.J.; Koutnik, J. The numerical simulation of the delayed load rejection of a pump-turbine power plant. In Proceedings of the 26th IAHR Symposium on Hydraulic Machinery and System, Beijing, China, 19–23 August 2012.
43. Chen, S. Investigation on 2-Stage Load Rejection and Water Hammer Protection in Hydroelectric Power Plants. Ph.D. Thesis, Hohai University, Nanjing, China, 12 September 2014.
44. Ghidaoui, M.S.; Zhao, M.; McInnis, D.A.; Axworthy, D.H. A Review of Water Hammer Theory and Practice. *Appl. Mech. Rev.* **2005**, *58*, 49–76. [[CrossRef](#)]
45. Yang, K.L. *Hydraulic Transient and Regulation in Hydropower Station and Pump Station*, 1st ed.; China Water & Power Press: Beijing, China, 1999.



© 2019 by the authors. Licensee MDPI, Basel, Switzerland. This article is an open access article distributed under the terms and conditions of the Creative Commons Attribution (CC BY) license (<http://creativecommons.org/licenses/by/4.0/>).